Chlorination of irradiated polyethylene single crystals: 1: Analysis of alkyl radical decay kinetics

H. J. Grimm* and E. L. Thomas†
Department of Chemical Engineering and Materials Science, University of Minnesota, Minneapolis, Minnesota 55455, USA
(Received 22 December 1983; revised 14 May 1984)

The chlorination of electron beam-irradiated polyethylene (PE) single crystals was studied for a range of irradiation doses, temperatures and chlorine interaction times. The results of this work are presented in two parts: (1) Electron paramagnetic resonance (e.p.r.) analysis of irradiated PE without chlorination and (2) characterization of chlorine uptake in irradiated PE by use of X-ray energy of spectroscopy (XES) and electron spectroscopy for chemical analysis (e.s.c.a.). Spectra were obtained for 75 – 600 Mrad doses over 136 to 333 K temperature range. Alkyl radical concentrations and decay kinetics were derived from e.p.r. spectra and provided a basis for the chlorination analysis in Part II. A first-order alkyl radical decay constant of $4.3\times10^{-5}s^{-1}$ at 298 K was determined in agreement with previous research. Alkyl radical migration was modelled as a one, two or three-dimensional unsteady-state Fickian diffusion process. E.p.r. alkyl radical concentration data was used to estimate alkyl radical diffusion coefficients yielding values of 10 to 4×10^{-18} cm^{2-1} at 298 K for the three models evaluated, respectively. These values are consistent with a diffusivity estimated by Seguchi and Tamura based on a 3-D model. A three-dimensional diffusion model seems to be the most realistic since it permits a zig-zag radical trajectory due to the staggered arrangement of $-CH_2-$ units in crystalline PE. Although a 3-D model would allow diffusion in all directions, it is still consistent with the observation that consecutive migration steps are most likely intermolecular.

(Keywords: chlorination; polyethylene; single crystals; alkyl radical decay; kinetics)

INTRODUCTION

Irradiation of linear polyethylene (PE) results in the generation of alkyl free radical centres. These alkyl radicals subsequently combine to form crosslinks and double bonds. Extensive crosslinking will eventually destroy the original crystal structure, yielding an amorphous, insoluble material. Although the details of radiation damage have been found to depend upon whether PE was crystallized from the melt or from dilute solution, the basic mechanisms of damage are the same.

PE crystal structure

Linear PE is a convenient polymer for study because of its simple crystal structure and the manner in which it crystallizes. Keller[1] was the first to explain PE crystallization in terms of chain folding, based on experiments of PE single crystals grown from dilute solution. PE crystals can be grown as diamond-shaped hollow pyramids with definite crystallographic growth faces. Electron microscopy revealed that solution-grown crystals were thin platelets ($\sim$100–300 Å thick) and that the polymer chain axis makes a large angle to the surfaces of the crystal platelet. Density and heat of fusion investigations of PE morphology indicate that less densely packed chain configurations are found in the surface regions. Priest *et al.*[2] estimated that the amorphous zone on each surface was approximately 10–15% of long spacing.

Effects of irradiation on crystalline PE: alkyl radical decay kinetics

It is believed that radical sites formed upon irradiation in the crystalline region migrate to the fold surface to either form conjugated double bonds or intermolecular or intramolecular crosslinks[2,8–11,17,30]. Charlesby[5], Dole *et al.*[6] and Lawton[7] concluded that crosslinking and increase in unsaturation via double bond formation are the predominant modes of physical damage in irradiated PE.

The chemically active sites, polymer free radicals formed by the loss of a hydrogen atom, can combine when they are in a favourable position (opposite each other on adjacent chains), to form a crosslink. The formation of a double bond can occur by the combination of radicals on adjacent sites of the same chain. Salovey and Keller[8] showed that crosslinks occur preferentially at the fold surfaces of lamellar crystals.

Three general types of free radicals have been detected in irradiated PE (in vacuum):

(1)	$-CH_2-\dot{C}H-CH_2$	alkyl radical
(2)	$-\dot{C}H-CH=CH-$	allyl radical
(3)	$-\dot{C}H-(CH=CH)_n-$	polyenyl radical

Electron paramagnetic resonance (e.p.r.), which measures the paramagnetism of the odd electron in a free

* Current address: Air Products and Chemicals, Inc., PO Box 538, Allentown, PA 18105, USA
† Current address: Dept. Polymer Science and Engineering, University of Massachusetts, Amherst, MA 01003, USA

0032-3861/85/010027-11$03.00

radical, has been used to (1) verify the presence of free radicals, (2) identify the free radical species, and (3) describe radical decay kinetics. Several studies[9-11] have demonstrated that the general radical decay scheme is one of alkyl free radicals decaying by combination to form crosslinks, double bonds and allyl and polyenyl free radicals. Alkyl radicals are stable at 77 K, but decay rapidly upon heating to room temperature. Initial alkyl radical population increases with increasing dose. Dole reported a radical concentration C_r of 5.2×10^{19} spins g^{-1} in PE single crystals irradiated to 30 Mrad at 77 K. This corresponds to one alkyl radical per 8 chain traverses, based on a 130 Å traverse consisting of approximately 100 $-CH_2-$ units. Dole and Waterman[12] observed that the alkyl radical concentration increases linearly with dose up to 80 Mrad at 77 K. At doses above 80 Mrad there is an increasing probability that combination of free radicals formed on adjacent sites will occur (even at 77 K). Thus, the measured radical concentration increases much less than linearly with increasing dose. Lawton *et al.*[9] found, for example, that the ratio of alkyl free radicals formed at 77 K for 320 and 40 Mrad was only 2.3.

Based on e.p.r. analysis of irradiated PE, Dole *et al.*[12,16-18] concluded that alkyl radical decay proceeded by first-order kinetics. Comparison of decay in amorphous and crystalline regions of PE revealed that decay proceeded more rapidly in the amorphous zones. Dole *et al.*[17] derived a kinetic scheme consisting of two different first-order alkyl radical decay processes occurring simultaneously: a fast decay rate in the amorphous region and a slow decay rate in the crystalline zones. Dole also showed that the presence of molecular hydrogen had a significant catalytic effect on both the fast and slow decay rates. As H_2 is only appreciably soluble in the amorphous zones, Dole suggested that the fast decaying radicals were all in the amorphous regions after warming from 77 to 298 K. Dole concluded that most, if not all, of the alkyl decay at and above room temperature must occur in the amorphous regions. A later decay study on irradiated freeze-dried PE single crystals yielded similar results[18]. As no H_2 solubility could be detected in the freeze-dried PE single crystals, the H_2 must have acted as a surface zone catalyst.

Seguchi and Tamura[27] measured alkyl radical decay (in air) of irradiated PE single crystals via e.p.r. and concluded that the behaviour of radical decay does not agree with the formula $dC/dt = KC^n$ ($n = 1$, 2, etc.). However, their data for $t > 2$ h, the time at which about 10% of the original radicals had decayed, is consistent with first-order kinetics, yielding a first-order constant of $K_1 = 2.4 \times 10^{-5}\ s^{-1}$ at 293 K.

Shimada, Hori and Kashiwabara[28] irradiated both PE single crystals and a urea–PE complex and claimed that alkyl radical decay could not be explained by using first-order kinetics over the entire radical lifetime. As with Seguchi's data, Shimada's decay data is approximately first-order after 10% of the orignal radicals had decayed. A first-order rate constant of $K = 8.5 \times 10^{-5}\ s^{-1}$ at 307 K can be calculated from Shimada's data for $t > 0.5$ h.

Dole, Keeling and Rose[6] first suggested that alkyl radical decay reactions occurred via migration of alkyl radical centres by a random walk process. The random walk is a means of explaining how alkyl radicals either reach double bonds to form allyl radicals or find other alkyl radicals with which to combine to form crosslinks or additional double bonds. This 'random walk' mechanism between energetically equivalent positions is one in which a hydrogen atom adjacent to a free valency centre shifts to the free valency centre while the latter makes the reverse shift to the site of the hydrogen atom. Numerous studies[9,10,13-15,27,28,30] have examined alkyl radical decay kinetics. One main conclusion of those studies is that migration occurs *across* adjacent chains rather than *along* the same chain, based on comparing the relative activation energies required[15].

Several of these studies have focused on whether the migration process is one, two or three-dimensional. It could be argued that migration can only be 1-D, across chains, since movement along the same chain is not energetically favoured. However, as Shimada *et al.*[28] pointed out, migration along the chain is possible through a certain set of two-step processes, chain A→chain B→ chain A. This is a mixed process of inter- and intramolecular migration, leading to a 3-D diffusion treatment. It is assumed that consecutive migration steps are intermolecular only.

Shimada's study of alkyl radical decay in a urea–PE complex seems to be strong evidence supporting intermolecular migration. In the urea–PE crystals, the molecules of PE are completely surrounded by urea molecules, and therefore, interchain migration of alkyl radicals is inhibited. Shimada's data shows that radical decay in the urea–PE complex is considerably slower than that in PE single crystals, implying intermolecular radical migration in pure PE.

The nature of alkyl radical migration has suggested that standard diffusion models could be applied to the data, and alkyl radical diffusion coefficients calculated. Seguchi and Tamura[27] examined both the 1-D and 3-D diffusion equations, based on radical diffusion from the crystalline interior to the fold surfaces, and concluded that the 3-D model better fit their decay data. Shimada *et al.*[28] applied the diffusion-controlled biomolecular reaction analysis first used by Waite[32] to calculate alkyl radical decay constants and diffusivities in both the amorphous and crystalline regions of PE. Shimada's treatment differs from Seguchi *et al.*[27] and Dole *et al.*[17] in that Shimada assumed that there is no communication between the radical populations in the crystalline and amorphous zones; that is, radicals are trapped in either the crystalline interior or amorphous surface and are only permitted to decay within their respective zones.

Effect of environment on irradiated PE

It is important to consider the effects of temperature and gaseous environment on irradiated PE. Irradiation of a sample at low temperature (77 K) will not prevent formation of radicals but only retard their decay. Higher temperatures enhance chain and radical mobility and thus increase the rate of radical decay. Most of the previous irradiation experiments have been conducted in vacuum in order to avoid carbonyl formation resulting from the following reaction:

$$O_2 + R\cdot \longrightarrow R\text{–}HC{=}O \qquad (1)$$

For years it has been known that oxygen acts as a radical scavenger. Few investigations have been conducted which concern the interaction of other gases with irradiated PE. One such study, however, was conducted by Dole *et al.*[6],

in which PE films were X-ray irradiated at room temperature and then exposed to bromine vapours in the dark at room temperature (as the dose rate was very low, the radical decay was probably complete before the bromine vapours were introduced). The purpose of these studies was to measure the extent of double bond formation via an addition reaction such as:

$$-HC=CH- + Br_2 \rightarrow -\underset{\displaystyle Br}{\overset{|}{HC}}-\underset{\displaystyle Br}{\overset{|}{CH}}- \qquad (2)$$

Comparison with infrared absorption measurements showed that the bromine uptake was about 2.6 times greater than the number of double bonds produced by irradiation, which probably indicates that the following substitution reaction also occurred:

$$-CH_2- + Br_2 \rightarrow -CHB'- + HBr \qquad (3)$$

Two other studies have been conducted which deal with the halogenation of unirradiated PE single crystals. In both studies the authors were interested in using chlorine or bromine as chemical probes for the study of the surface structure of PE single crystals.

Keller[19] brominated a suspension of PE crystals under incandescent light for 24 h. Upon filtering and drying, it was observed that the crystals melted at 401 K, 8 K lower than the melting point of the unbrominated polymer. Chemical analysis showed that after reaction, the polymer had a bromine content of 4.5% by weight or one bromine atom per long spacing. When the brominated crystals were recrystallized, their fold length (long spacing) remained constant. Keller also chlorinated PE, comparing chlorine uptake in single crystals and bulk PE at several temperatures. These reactions were promoted by either light or heat. The general halogenation scheme is outlined below:

(1) Initiation

$$X_2 \xrightarrow{\text{u.v. or heat}} 2X\cdot$$

(2) Chain propagation

$$X\cdot + RH \rightarrow HX + R\cdot$$
$$R\cdot + X_2 \rightarrow RX + X\cdot$$

(3) Termination

$$R\cdot + R\cdot \rightarrow R\text{–}R$$
$$X\cdot + X\cdot \rightarrow X_2$$
$$R\cdot + X\cdot \rightarrow RX$$

where X is a halogen atom (F, Cl, Br, I). At room temperature under incandescent light a maximum increase of only 3.5% by weight was obtained, corresponding again to one chlorine in 73 atoms or about one chlorine atom per long spacing. Due to the assumed impenetrability of the crystal lattice at room temperature, chlorination was believed to occur only in the amorphous surface zones.

Chlorination at elevated temperatures (333 and 353 K) produced entirely different results. Chlorine uptake as measured by weight gain at 333 and 353 K after 24 h was 97 and 158%, respectively. For the latter uptake this corresponds to one chlorine for every 1.4 carbon atoms.* When a highly chlorinated sample (weight increase of 97%) was dissolved and recrystallized, only part of the sample precipitated in the form of well defined single crystals, the remainder giving a poorly defined, shapeless precipitate. By studying the diffraction pattern of the chlorinated product, Keller showed that the chlorine reacted with the original crystalline lattice until it was completely destroyed; that is, the resulting diffraction pattern (5.8 Å ring) resembled that of vinyl polymers with a high chlorine content, but the 5.8 Å spacing corresponded neither to polyvinyl chloride nor to polyvinylidene chloride.

Harrison and Baer[21] conducted PE bromination experiments and showed two effects: firstly, bromination takes place preferentially at the fold surfaces and is consistent with a regular adjacent reentry fold model, and secondly, that annealing of those brominated crystals demonstrates the major role played by the crystal surface in the annealing process. As in Keller's experiments, halogenation was initiated by ultraviolet light and the maximum uptake was 1 halogen atom per long spacing.

Quenum *et al.*[22] investigated PE chlorination by infrared analysis. High and low density PE specimens were either photo or thermally chlorinated up to 73% chlorine by weight. From infrared analysis, chlorine peaks were assigned to the 660 cm^{-1} band. Other results were concerned with changes in the molecular structure of the chlorinated PE samples during the chlorination process.

In another halogenation study, Margrave *et al.*[23] observed that PE could be fluorinated without initiators at room temperature simply by flowing a stream of fluorine gas (F_2) over finely dispersed powdered PE which was initially in a vacuum. These samples were in the form of powders in order to avoid F_2 diffusion limitations. Margrave reported that the reaction:

$$-H_2C\text{–}CH_2- + F_2 \xrightarrow{293\ K} -F_2C\text{–}CF_2- \qquad (4)$$

was essentially complete within 24 h. Unfortunately, Margrave *et al.* did not explain why PE fluorination occurred in the absence of initiators. As fluorine is more reactive than chlorine, it is not clear whether PE samples can be likewise chlorinated in the absence of initiators at room temperature, although the work of Keller would seem to indicate that little chlorination would take place without an initiator such as u.v. light.

In this research, the interaction of chlorine gas with irradiated PE was studied. One difference between these halogenation reactions and those of Keller *et al.*[19] was that these chlorination reactions were not initiated by ultraviolet light. Instead, free radicals were formed via electron beam irradiation. Chlorine gas was then introduced, resulting in chain reactions (propagation) (5) and (6) as shown below:

$$R\cdot + Cl_2 \xrightarrow{E_{a1}} RCl + Cl\cdot \qquad (5)$$

$$Cl\cdot + R'H \xrightarrow{E_{a2}} HCl + R'\cdot \qquad (6)$$

* Peterlin *et al.*[20] also observed significant halogen (I_2 vapours) solubility in the crystalline regions of polyethylene at and above 333 K

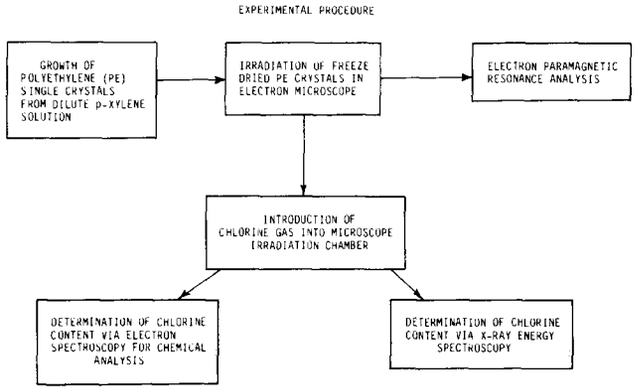

Figure 1 Experimental procedure

where the activation energies E_{a1} and E_{a2} are approximately 0.1 and 0.3 kcal mol^{-1}, respectively. Termination reactions (such as those presented in the general halogenation scheme) would only take place when the number of available chlorination sites approaches zero, probably after significant chlorne uptake has occurred. Chlorine gas would also be expected to react with any double bonds formed during irradiation, as shown in reaction (7):

$$Cl_2 + -CH{=}CH- \xrightarrow{*E_{a3}} \underset{Cl\ Cl}{HC{-}CH-} \qquad (7)$$

which is similar to that observed by Dole *et al.*[6] in the bromination of irradiated PE films.

EXPERIMENTAL TECHNIQUES

Figure 1 shows an outline of the experimental procedure and techniques used in this research. Details of the procedure are described in the following sections.

Growth of PE single crystals

A modified 'self-seeding' procedure described by Harrison and Baer[21] was used to grow PE crystals at 358 K in a dilute (0.2% weight) *p*-xylene solution. Marlex® 6009 PE was used exclusively in this work ($M_w = 136\,000$ $M_w/M_n = 13.4$).

Freeze-drying of PE single crystals

Freeze drying is preferable to filtering due to its greater efficiency in exposing the maximum surface area/weight. Filtration causes caking and a great variation in sample thickness. The freeze drying technique consists of first removing excess solvent, freezing the solution, and then drawing off the solvent via sublimation. In this work, PE single crystals were grown in *p*-xylene, frozen by placing the vessel in liquid nitrogen and then dried by attaching under vacuum for approximately 24 h. The dried crystals were powdery and fluffy in appearance. *p*-Xylene was chosen (over a blend of xylene isomers) because of its high freezing point, 285 K.

* Although a value E_{a3} has not been reported, reaction (7) has been observed to occur readily at room temperature[24]

Irradiation and chlorination of PE single crystals in transmission electron microscope (TEM)

An RCA 100 KV TEM was used as the irradiation source in this study. Use of an electron accelerator was preferred over a γ-ray facility because the TEM could deliver up to several megarads (Mrad) dose per minute. Irradiation was accomplished by placing ~0.01 g of the freeze-dried PE crystals in a chamber which was attached below the camera section of the microscope. This irradiation chamber, shown in *Figure 2*, consisted of a specimen chamber which was attached to a teflon gate valve housing. When the gate valve was open, the sample could be electron-beam irradiated. After irradiation, the gate valve was closed to permit introduction of chlorine gas only into the specimen chamber. A constant chlorine gas pressure of ~0.2 Torr was maintained during all chlorination experiments, measured by a thermocouple vacuum gauge located below the gate valve. Irradiation temperature was varied by immersing the specimen chamber in a temperature bath. After nitrogen-purging chlorine from the specimen chamber, the sample was removed, a new sample inserted, the teflon gate valve reopened, the system brought to high vacuum (10^{-6} Torr) and the irradiation–chlorination procedure repeated. The microscope was returned to normal use by removing the irradiation chamber.

Determination of irradiation dose

Dose measurements were made for absorbed dose which is expressed in rad, where:

$$1\ \text{rad} = 100\ \text{erg/g}$$

of energy absorbed by the sample during irradiation. A dose of 4000 Mrad (4×10^9 rad) completely destroys the crystal structure in PE as observed by loss of the diffraction pattern. Absorbed dose was conveniently measured in the microscope by use of a Faraday cup which measured the beam current.

The Faraday cup fabricated for this study was a modification of a design employed by Grubb[26]. The cup

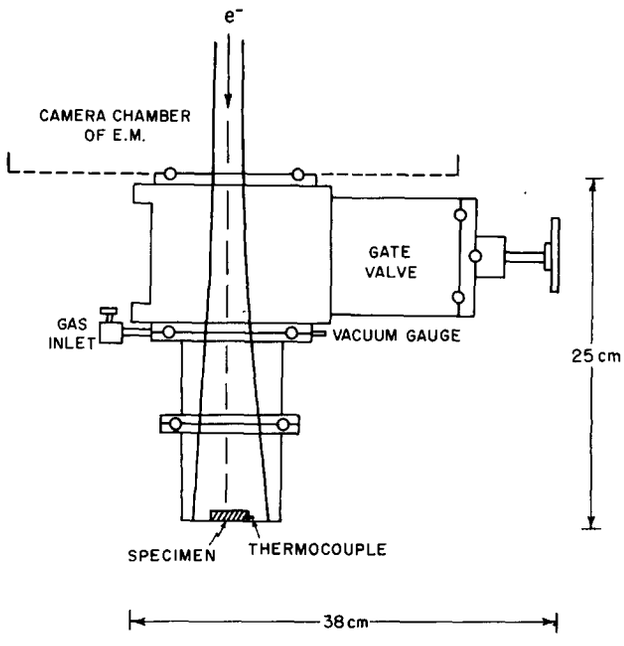

Figure 2 Irradiation chamber for the electron microscope

Table 1 Dose rates employed in irradiation of PE single crystals

Current i (amp x 10^7)	Time t (min)	Dose D (Mrad)	Dose rate (Mrad^{-1})
1.4	3	1	20
21	8	38	285
20	17	75	265
120	23	600	1505

was designed to fit into the conventional TEM specimen chamber which acted as an earthed shield as well as helping align the cup aperture with the beam. Current was measured with a Keithley model 610B electrometer. Absorbed dose D is then given by:

$$D = it/A \tag{8}$$

where i = beam curreng (amp), t = irradiation time (s), and A = irradiated area (cm^2). Equation (8) indicates that the dose D is directly measured as current flux (amp − s cm^{-2}). Grubb and Keller[25] give, based on PE:

$$1 \text{ amp} - \text{s cm}^{-2} = 4 \times 10^5 \text{ Mrad}$$

as a reasonable estimate for the conversion of amp − s cm^{-2} into rad for 100 kV irradiation.

The irradiation area (10.9 cm^2) was set at approximately twice the specimen cup area to ensure even irradiation of the sample and to minimize collision of the electron beam with the chamber walls (see *Figure 2*).

The currents and times required to achieve the irradiation doses employed are given in *Table 1*. The electron beam current was increased as the dose increased in order to minimize the irradiation time. Thus the dose rates given above are quite large compared to those achieved by use of γ-ray irradiation (less than 1 Mrad h^{-1}). Dose measurements employing Faraday cup were in error by $\pm 4\%$, $\pm 5\%$ and $\pm 11\%$ for 1, 75 and 600 Mrad, respectively. The main source of error in dose determination was that in measuring the irradiation area which varied by $\pm 10\%$.

Electron beam penetration and XES and e.s.c.a. sampling depth problems were overcome by mounting PE single crystals in scanning microscope (SEM) sample stubs that had been modified to hold the crystals. The crystals were then irradiated, chlorinated and then analysed via XES and e.s.c.a. without need for removal. In this way, XES and e.s.c.a. analysed an approximately homogeneously irradiated and chlorinated sample, since the 20 kV beam used in XES penetrates to 6 μm and the analysis depth for e.s.c.a. is only 20–30 Å, compared to the 40 μm depth of nearly constant (within 10%) energy deposition of a 100 kV electron beam (electron range depth $\simeq 65$ μm).

Temperature measurement

Sample temperature was measured via a copper constantan thermocouple located at the bottom of the irradiation chamber. Cold temperatures were achieved by use of liquid nitrogen (77 K), acetone-dry ice (232 K), and sodium chloride–ice water mixtures (252 K). Room temperature varied in the range 298–300 K. Higher temperatures were obtained by use of an ethylene glycol bath.

Use of electron paramagnetic resonance

A Varian E-3 Electron Paramagnetic Resonance instrument operating at a microwave frequency of 9.15 GHz was used as a means of identifying the radical type, their concentrations, and decay kinetics. This instrument was used to study irradiated PE crystals that had not been chlorinated. A minimum of 10^{13} spins (i.e. radicals) was the detection threshold of the instrument. The spectra were typically recorded in the vicinity of 3.2 kGauss with the modulation amplitude at 4 Gauss or less. About 0.005 g sample irradiated to 75 Mrad gave a strong signal.

Determination of chlorine content via XES

X-ray Energy Spectroscopy (XES) was employed in order to determine the amount of chlorine present in the irradiated–chlorinated PE samples. This was the first study to be conducted using XES analysis on irradiated–chlorinated PE. The method consists of scanning an electron beam over an area of interest, thus producing characteristic X-rays, and then collecting these X-rays by an X-ray detector. Samples were scanned in a Cambridge scanning microscope at 20 kV and 200× magnification over an area of approximately 2.6×10^{-4} cm^2. The X-rays produced from the sample strike the detector crystal producing charge pulses which are proportional to their energies. These pulses or counts are then sorted into channels by the spectrometer which integrates the counts collected in a given energy region ('window') of interest over time. The scan time chosen was 100 s. The data collected for a given window consisted of a net count (peak − background) and a gross count (peak + background). By choosing an energy window corresponding to a given element one can determine the relative amount of that element present. In this case the element of interest was chlorine. The chlorine window was set to 2.36–2.89 keV and another window was set for 0.5–10.24 keV to collect chlorine and other X-rays from the sample. If P_1 is the net counts from the chlorine window and P_2 the gross counts from the larger window, then:

$$P_1/P_2 = c_1 = \frac{\int_{2.36}^{2.89} \text{Cl} - \int_{2.36}^{2.89} \text{background}}{\int_{2.36}^{2.89} \text{background}}$$

c_1 gives a relative measure of chlorine present but not the % chlorine present in the sample. Poly(vinylchloride) (PVC) was used as a reference in order to calculate the % chlorine in the chlorinated samples. It is known that PVC is 25% chlorine by number of sites and from XES data for PVC:

$$P_1'/P_2' = c_1$$

and likewise for chlorinated PE:

$$P_1/P_2 = c_2$$

then to find the chlorine fraction X_{Cl}:

$$X_{Cl} = c_2(0.25/c_1) \times 100 = \% \text{ chlorine in the sample}$$

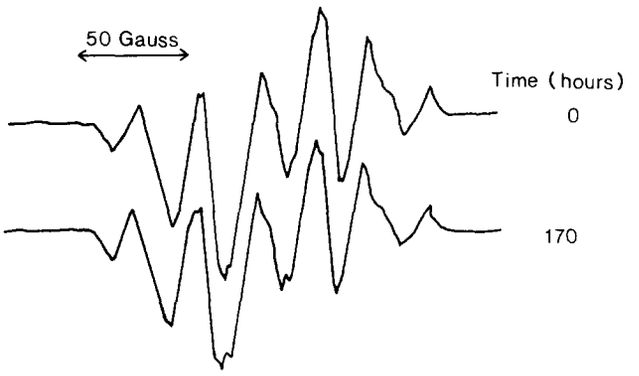

Figure 3 E.p.r. spectra of polyethylene single crystals irradiated to 120 Mrad at 136 K (e.p.r. conducted at 136 K)

XES analysis was conducted for three different areas on each sample, averaging the number of counts in order to obtain an X_{Cl} value. The number of pulses counted did not vary by more than $\pm 3\%$ from one sample area to the next.

Determination of chlorine content via e.s.c.a.

A Physical Electronics ESCA instrument was employed in order to obtain chlorine content values for comparison purposes with XES. The main difference between the two methods is that e.s.c.a. is only surface sensitive (sampling 20–30 Å depth) whereas XES analyses to ~ 6 μm of sample depth (dependent on incident beam energy employed). E.s.c.a. experiments consisted of bombarding the samples with $Mg_{K\alpha}$ X-rays, generating secondary electrons whose energies are characteristic of the element from which they were ejected, then sorting these electrons according to energy by use of an electron spectrometer. A gold sample was used in calibrating the e.s.c.a. instrument. E.s.c.a. analysis was conducted in a vacuum of 10^{-8} Torr. Irradiated–chlorinated PE single crystals mounted on modified SEM sample stubs for e.s.c.a. analysis were the same as those studied via XES. As before, PVC was used as a reference in calculating chlorine content. The C_{1s} and Cl_{2p} peaks were of main interest here. The presence of silicon and oxygen was due to surface contamination. As the sample orientation, etc. can vary upon changing specimens, chlorine peak heights were always expressed relative to those of carbon as a means of normalizing the data. E.s.c.a. peak heights for each element present were adjusted to account for differences in electron excitation efficiencies. It was possible to remove portions of the sample surface by argon ion sputter etching in order to measure the chlorine content in sample regions located at original depths greater than 30 Å.

RESULTS AND DISCUSSION

E.p.r. results obtained were similar to those observed by previous researchers[12,16,20]. E.p.r. spectra were obtained for doses of 75–600 Mrad and temperatures ranging from 136 to 333 K. At 136 K only the alkyl radical was observed, as characterized by the six-line spectra obtained in *Figure 3* for PE irradiated to 120 Mrad. *Figure 3* is based on a one-week study in which an irradiated PE sample was maintained at 77 K between measurements and at 136 K during e.p.r. measurements. There was no measurable difference in spectra at times $t=0$ and $t=170$ h as seen in *Figure 3*, indicating that alkyl radicals are quite stable at this temperature. Numerous researchers observed similar alkyl radical stability at low temperatures. PE irradiated at 298 K, however, yields alkyl radicals which quickly decay to allyl and polyenyl radicals. Dole *et al.*[16] showed that $\sim 70\%$ of the alkyl radicals generated during irradiation at 77 K decayed upon heating to 298 K (~ 10–15 min later). The remaining 30%, referred to as 'residual' alkyl radicals[16], decay quite slowly at 298 K, with a half-life of ~ 5 h. Since the residual radicals decay slowly at 298 K, it was assumed that 30% of the initial alkyl radical population would be present at $t=0$ (time at which irradiation was complete). Similarity of the detail of the e.p.r. spectra obtained for 136 and 298 K (at $t=0$) shown in *Figures 3* and *4* indicate that there was probably no significant residual alkyl radical decay during irradiation at 298 K.

Alkyl radical concentration

E.p.r. was used in this work to determine the alkyl radical concentration as a function of dose ($C_r(D)$). $C_r(D)$, expressed in No. radicals/traverse,* was calculated by combining the alkyl radical concentration vs. dose data of Dole and Wen[16] with the e.p.r. spectra in *Figures 4* and *5*. As the first peak of the e.p.r. spectra (marked 'A' in *Figures 4* and *5*) is unique to the alkyl radical signal[12], comparison of the first peak heights at time $t=0$ for different doses would give a relative measure of the initial (residual) alkyl radical concentrations. Dole found that the alkyl radical concentration at time $t=0$ (after irradiation at 77 K) increased linearly with dose for doses up to approximately 80 Mrad. In that study, Dole[16] reported an alkyl radical concentration value $C_r(30)=5.2\times10^{19}$ spins/g† at 30 Mrad and 77 K. This corresponds to about 1.25 spins/10 traverses for the 130 Å long period PE single crystals used here. Extrapolation of the $C_r(30)$ value

* Where 1 traverse = 1 long spacing = 130 Å = 103 $-CH_2-$ units for the PE crystals used in this work

† 1 spin = 1 alkyl radical

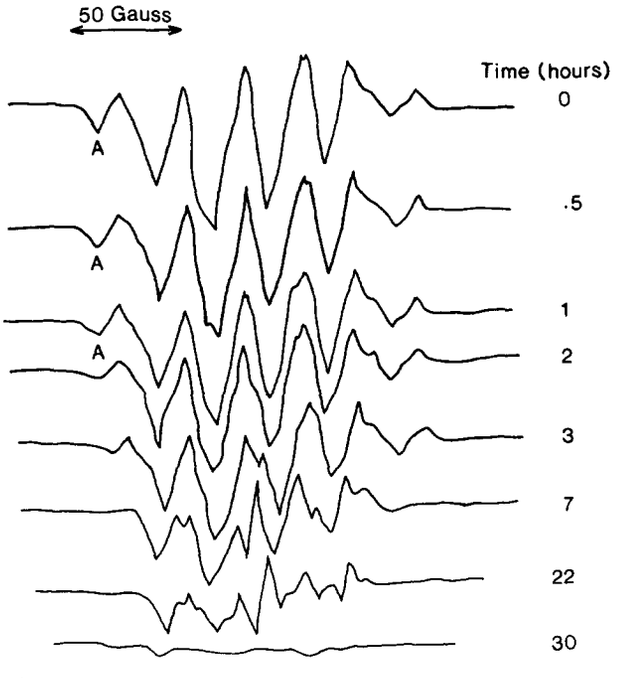

Figure 4 E.p.r. spectra of polyethylene single crystals irradiated to 75 Mrad at 298 K (e.p.r. conducted at 298 K)

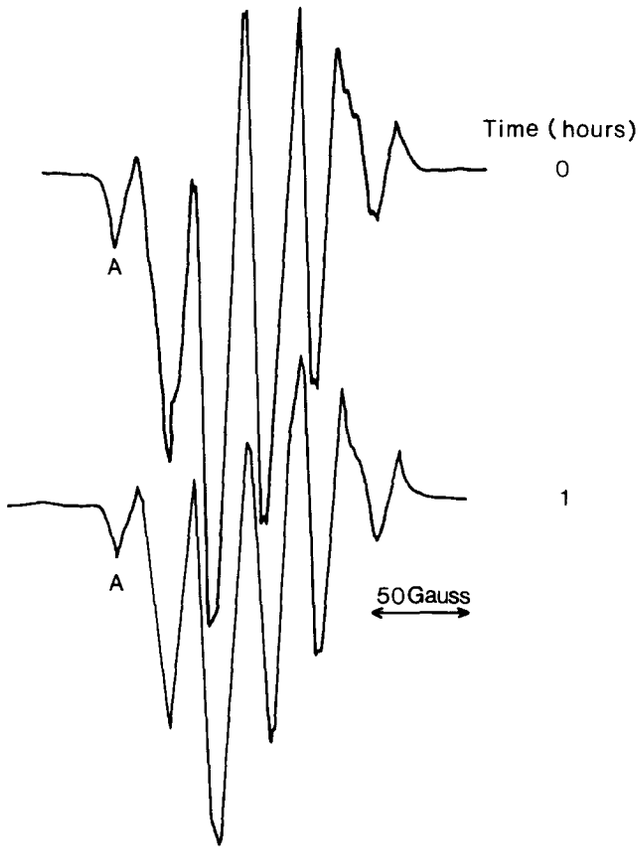

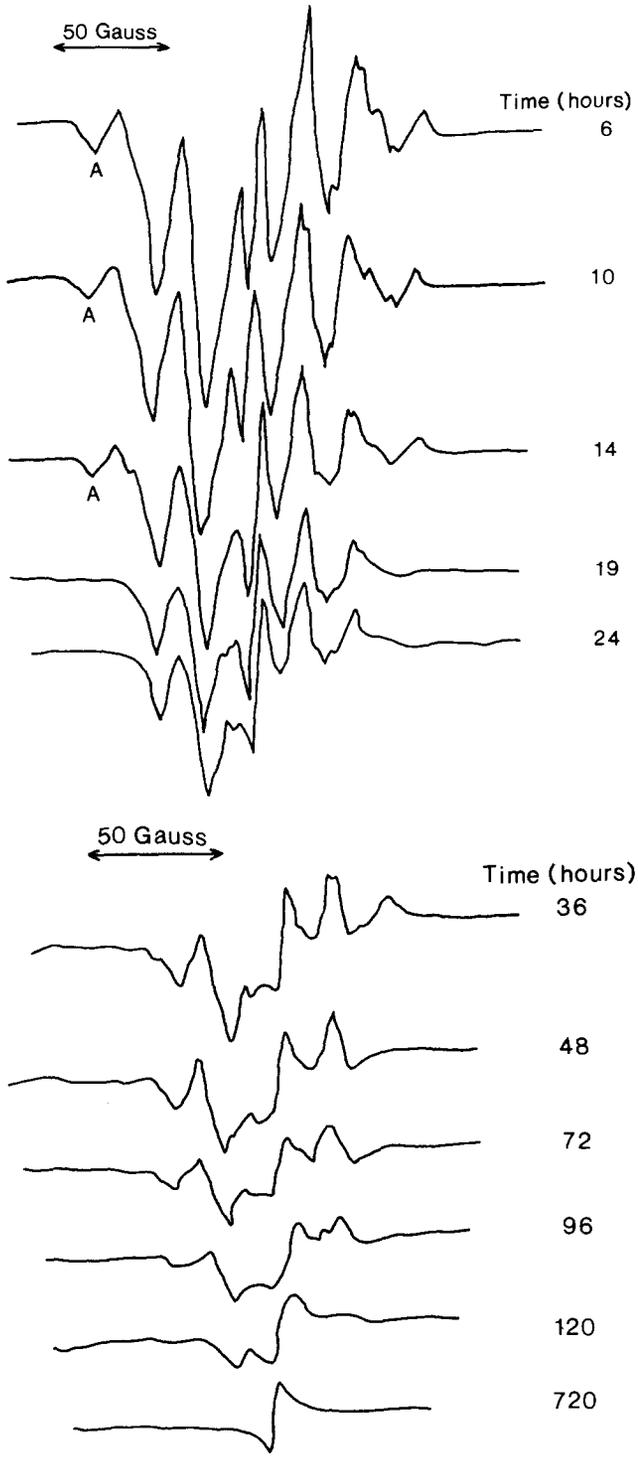

Figure 5 E.p.r. spectra of polyethylene single crystals irradiated to 600 Mrad at 25°C (e.p.r. conducted at 298 K)

to 75 Mrad yielded $C_r(75) = 3.1$ spins/10 traverses. As discussed previously, 70% of the initially formed alkyl radicals decay upon warming to room temperature (or during high dose rate-irradiation at room temperature). Therefore, the residual alkyl radical concentration $C'_r(75) = 0.9$ spins/10 traverses.

At doses above 80 Mrad there is an increasing probability that combination of free radicals will occur during irradiation and thus the measured radical concentration ($C'_r(D)$) increases much less than linearly with increasing dose[12]. This phenomena can be seen here by comparing the first peak (A) heights of the e.p.r. spectra at time $t = 0$ for 75 and 600 Mrad (see *Figures 4* and *5*). The ratio of these peak heights at time $t = 0$ indicates that the residual alkyl radical concentration at 600 Mrad is only four times that at 75 Mrad. Thus $C'_r(600)$ is approximately 3.6 spins/10 traverses. Comparison of the first peak heights from the e.p.r. spectra at 75 and 1000 Mrad (the 1000 Mrad spectra are not shown here) indicated that the alkyl radical concentration at time $t = 0$ for this high dose is only 4.4 times that of the lower dose. The alkyl radical concentration data obtained in this research are summarized in *Table 2*. The $C_r(D)$ values listed above refer to the alkyl radicals formed during irradiation and the $C'_r(D)$ values correspond to the alkyl radicals which remain at the time of the first e.p.r. measurement ($t = 0$).

Alkyl radical decay kinetics

From e.p.r. spectra it was possible to determine the relative change in alkyl radical concentration by measuring the change in the height of the wing peak (first peak) of the e.p.r. spectra for a given dose. Balwitt[9] observed that as the alkyl radical population decreased to zero, the first

Table 2 Alkyl radical concentration as a function of dose

Dose (Mrad)	Irradiation at 298 K Relative first peak height (t = 0)	$C_r(D)$ (77 K) no. spins/10 traverses	$C'_r(D)$ (298 K) no. spins/10 traverses
75	1	3.1	0.9
600	4	25	3.6
1000	4.4	42	4.0

peak height also fell to zero. Since the e.p.r. signal from the coexisting alkyl radials does not overlap with the wing peak, the diminishing of the first peak over time is a good measure of alkyl decay.

Figure 6 is a plot of the relative alkyl radical concentration C/C_0 vs. time at 298 K based on the decrease of the wing peak (marked A in *Figure 5*) of the e.p.r. spectra over time for PE single crystals irradiated to 600 Mrad. A first-order rate constant $K_1 = 4.3 \times 10^{-5}\ s^{-1}$ at 298 K was determined from *Figure 6*. *Figure 6* also indicates that the residual alkyl radical half-life ($C/C_0 = 0.5$) was ~4.4 h at 298 K. Decay data in *Figure 6* is compared to that obtained by Seguchi and Tamura[27], Shimada *et al.*[28] and Dole *et al.*[12,16] in *Table 3*. Although the Seguchi and Shimada data was not consistent with first-order kinetics for small time, their data satisfactorily represented first-order decay for $t > 0.5$ h (Shimada) and $t > 2$ h (Seguchi). In

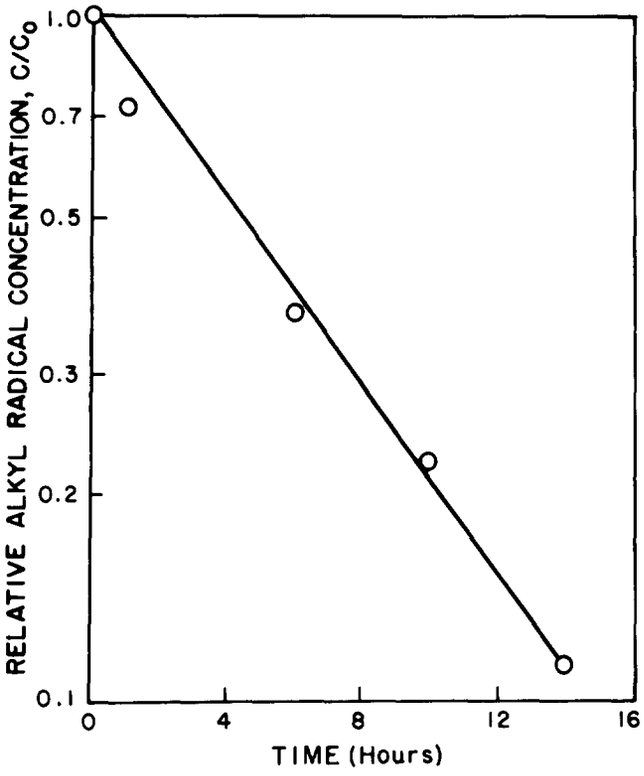

Figure 6 Alkyl radical decay at 298 K in polyethylene single crystals irradiated to 600 Mrad

the Dole *et al.* work[12,16], a detailed kinetic analysis yielded a method for separately determining both fast decaying radicals (radicals which have already migrated into the amorphous zones) and slow decaying radicals (radicals which are in the crystalline regions, migrating towards the amorphous surface zones). Dole's $K_s = 1.02 \times 10^{-5}\ s^{-1}$ (slow radicals) and $K_f = 1.85 \times 10^{-4}\ s^{-1}$ (fast radicals) at 298 K is consistent with the $K_1 = 4.3 \times 10^{-5}\ s^{-1}$ at 298 K reported in this study, which is a composite of the slow and fast decaying radicals.

To compare Seguchi's and Shimada's rate constants to Dole's and the value obtained here, it is necessary to correct their rate constants to 298 K. Dole, Waterman and Wen[17] derived an Arrhenius equation for alkyl radical decay in both the amorphous and crystalline regions, showing that the activation energy in both regions is the same, but the preexponential factor for the amorphous zone is much larger than that for the crystalline zone. Use of their Arrhenius equation to determine ratios of rate constants at different temperatures shows that the K_1 values given in *Table 3* are consistent; that is, the values only differ due to temperature.

Alkyl radical diffusivity

The nature of alkyl radical site migration to the fold surface zone and subsequent combination there suggests that the migration process could be modelled similarly to the case in which a gas-saturated film is placed in a vacuum at time $t = 0$. In the film problem, the gas molecules diffuse to the surfaces of the film and escape. Analogously, alkyl radical sites migrate to the fold surface and combine. As the gas diffusion case has been modelled as an unsteady-state diffusion process, alkyl radical site migration can be similarly modelled.

Unsteady-state one, two and three-dimensional diffusion models and the alkyl radical decay data (from *Figure 6*) were used to estimate alkyl radical diffusion coefficients at 298 K. The following assumptions were incorporated into the three models considered:

(1) Alkyl radical site migration is described by Fick's First Law of Diffusion.

(2) The effective diffusion path length, l for the various dimensional models can be estimated by considering the morphology of PE single crystals (see *Figure 7*). The radical sites migrate until they reach the amorphous fold

Table 3 Comparison of alkyl radical decay data for irradiated PE single crystals

Source of data	T_c Polyethylene crystallization temp. (K)	L Long period (Å)	T Radical decay temp. (K)	Environmental of sample	$t_{1/2}$† Alkyl radical half-life (10^3 s)	K First-order alkyl radical decay constant ($10^{-5}\ s^{-1}$)
Grimm–Thomas	358	130	298	vacuum	15.8	4.3
Seguchi–Tamura[27]	358	123	293	air	36.0	2.4§
Shimada *et al.*[28]	358	130‡	307	vacuum	6.3	8.5*
Dole *et al.*[12,16]	363	–	298	vacuum	–	1.02** (slow)
						18.5 (fast)

†$t_{1/2}$ = alkyl radical half-life, time at which $C/C_0 = 0.5$
$t_{1/2}$ for Seguchi and Shimada *et al.* are based on the radical populations which exhibited first-order kinetics
‡L data not given, L = 130 Å was assumed
§for $t > 2$ h
*for $t > 0.5$ h
**K values from Dole *et al.* data were calculated using an Arrhenius equation derived by Dole *et al.*[16] for the fast and slowly decaying alkyl radicals

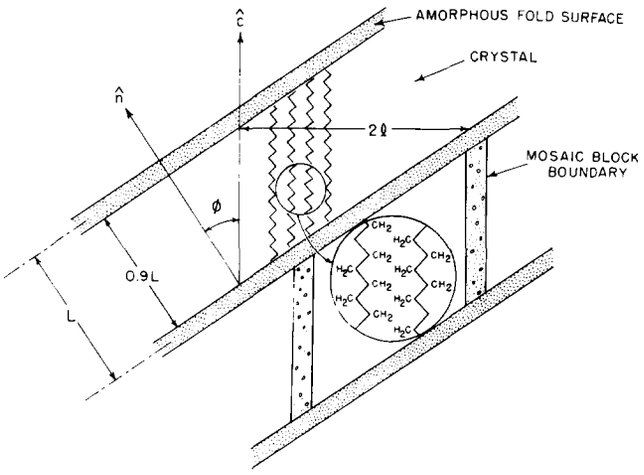

Figure 7 Schematic of hollow pyramidal PE single crystal showing alkyl radical migration path length l across chain stems

surfaces or encounter a defect boundary region between crystals (mosaic block boundaries[31]). In *Figure 7*, ϕ is the chain inclination angle between the normal to the lamellar surface ($\hat{n}$) and the chain axis ($\hat{c}$), L is the long period and l_c is the crystal thickness (taken as $l_c = 0.9\,L$). In this study, $L = 130$ Å and $\phi = 40°$ was used, based on published data[29,33] for PE single crystals grown in xylene at 358 K. From the geometry of *Figure 7*, l is given by:

$$l = \frac{0.9\,L}{2\sin\phi} \tag{9}$$

which yields a value of 9.1×10^{-7} cm (91 Å). The value ($2l$) is comparable to typical (~300 Å) mosaic block sizes measured by X-ray scattering. Since CH_2 units on adjacent chains are staggered along $\hat{c}$, radical site migration across chains can result in net radical movement parallel to $\hat{c}$. Hence along $\hat{c}$, the effective diffusion path length is approximately $0.9\,L/2\cos\phi$ which is sufficiently close to l to assume the effective 1-D, 2-D and 3-D diffusion path lengths are all just l.

(3) *Initial condition*: the alkyl radical population is uniformly distributed at time $t = 0$ (C_0).

Boundary condition: alkyl radical sites immediately combine at the fold and/or mosaic block surfaces; that is, $C(\pm l, t) = 0$ for time $t > 0$, where l is the diffusion path length. It is also assumed that a negligible number of the radicals combine in the crystal interior.

(5) Alkyl radical diffusion coefficients, D_a are estimated by evaluating the appropriate model at the radical half-life condition, employing the kinetic data in *Figure 6* at $C/C_0 = 0.5$. D_a is back-calculated by using the following expression:

$$\bar{C}(t_{1/2}) = \frac{C_0}{2} = 0.5 = \frac{\int_0^l C(x,t_{1/2})x}{\int_0^l \mathrm{d}x} \tag{10}$$

where $\bar{C}(t_{1/2})$ is the average radical concentration at the half-life and $C(x,t_{1/2})$ is the analytical expression for alkyl radical concentration obtained from the model at the half-life. *Figure 6* indicates that $t_{0.5} = 4.4$ h.

1-D model

This model assumes radical migration is a strictly intermolecular straight line path normal to the chain backbone. The one-dimensional unsteady-state diffusion equation is given by:

$$\frac{\partial C}{\partial t} = D_a \frac{\partial^2 C(x,t)}{\partial x^2} \tag{11}$$

where $C(x,t)$ is the alkyl radical concentration at position x and time t. Solving equation (11) using the initial and boundary conditions given above yields:

$$C(x,t) = \frac{4C_0}{\pi} \sum_{m=0}^{\infty} \frac{(-1)m}{(2m+1)} \cos\left[\frac{(2m+1)\pi x}{2l}\right] \exp\left[\frac{-D_a(2m+1)^2\pi^2 t}{4l^2}\right] \tag{12}$$

$(D_a)_{1-D}$ is estimated from the half-life data using the following expression derived from equation (10):

$$(D_a)_{1-D} = 0.1958\frac{l^2}{t_{1/2}} \tag{13}$$

From *Figure 6*, $t_{1/2} = 1.58 \times 10^4$ s (4.4 h) at $C/C_0 = 0.5$. Substitution of these values into equation (13) yields $(D_a)_{1-D} = 1.03 \times 10^{-17}$ cm^2 s^{-1}.

2-D model

Two-dimensional unsteady-state diffusion is modelled by:

$$\frac{1}{D_a}\frac{\partial C(r,t)}{\partial t} = \frac{\partial^2 C(r,t)}{\partial r^2} + \frac{1}{r}\frac{\partial C(r,t)}{\partial r} \tag{14}$$

Equation (14) is solved using the initial and boundary conditions given above to yield:

$$C(r,t) = \sum_{n=1}^{\infty} \frac{2}{(\lambda_n R)J_1(\lambda_n R)} J_0(\lambda_n r) e^{-(D_a\lambda_n^2 t)} \tag{15}$$

where λ_n are the roots of $J_0(\lambda_n R) = 0$ and $R = l$ is the radius of a cylinder surrounded by amorphous zones (radical sink). $(D_a)_{2\text{-D}}$ is estimated from the half-life data using the same procedure as for the 1-D model, yielding the following:

$$(D_a)_{2\text{-D}} = 0.1157\frac{R^2}{t_{1/2}} \tag{16}$$

Evaluation of equation (16) gives $(D_a)_{2\text{-D}} = 6.1 \times 10^{-18}$ cm^2 s^{-1} at 298 K.

3-D model

This model permits diffusion along $\hat{c}$ by a mixed inter–intra molecular process in addition to motion normal to $\hat{c}$. The three-dimensional unsteady-state diffusion equation is given by:

$$\frac{\partial C(r,t)}{\partial t} = D_a\left(\frac{\partial^2 C(r,t)}{\partial r^2} + \frac{2\partial C(r,t)}{r\partial r}\right) \tag{17}$$

Table 4 Summary of alkyl radical diffusivities in PE single crystals

	D_a in crystalline region (units of 10^{-17} cm^2 s^{-1})				
	T (K)	Previously reported value	Calculated Grimm–Thomas 1-D model	Calculated Grimm–Thomas 2-D model	Calculated Grimm–Thomas 3-D model
Grimm-Thomas	298	–	1.03	0.61	0.435
Seguchi[27]	293	0.3	0.54	0.32	0.23
Shimada[28]	307	0.00011†	2.57	1.52	1.1

†Shimada *et al.*[28] reported $D_a = 1.1 \times 10^{-21}$ cm^2 s^{-1} for alkyl radicals in the crystalline regions and $D_a = 9 \times 10^{-20}$ cm^2 s^{-1} for radicals in the amorphous zones. The comparisons here are based on D_a in the crystalline regions

As before, initial and boundary conditions are employed to solve the differential equation, giving:

$$C(r,t)=\frac{2RC_0}{\pi r}\sum_{n=1}^{\infty}\frac{(-1)^{n+1}}{n}e^{D_a n^2\pi^2 t/R^2}\sin\left[\frac{n\pi r}{R}\right] \quad (18)$$

where $R=l$ is the radius of a sphere surrounded by amorphous zone radical sinks (fold surfaces and mosaic block boundaries). A $(D_a)_{3\text{-D}}$ value of 4.35×10^{-18} cm^2 s^{-1} was back-calculated using the following implicit expression derived from the half-life condition, based on the first three terms of the series solution:

$$0.5=1.1794\exp\left[-9.87\frac{D_a t_{1/2}}{R^2}\right]-0.4543$$
$$\exp\left[-39.48\frac{D_a t_{1/2}}{R^2}\right]+0.4255\exp\left[-88.83\frac{D_a t_{1/2}}{R^2}\right] \quad (19)$$

The 3-D model appears to be the most realistic as it permits a zig-zag radical trajectory due to the staggered $-CH_2-$ units (*Figure 7*) incorporating the possibility of a net intramolecular migration via a chain A→chain B→ chain A type process.

Diffusivities determined in this study are listed in *Table 4* and compared to values reported by Seguchi and Tamura[27] and Shimada *et al.*[28]. Since the same diffusion path length (l) was used to estimate alkyl radical diffusivity in the 1-D, 2-D and 3-D models, the D_a values listed in *Table 4* rank as $(D_a)_{1\text{-D}}>(D_a)_{2\text{-D}}>(D_a)_{3\text{-D}}$. Shimada's and Seguchi's kinetic data were used to compute D_a values for the 1-D, 2-D and 3-D models and are listed in *Table 4*. The similarities in the calculated D_a values using the three kinetic data bases (taking into account the effect of temperature) are contrasted to the relatively large differences between the D_a values reported by Seguchi and Shimada. Apparently, the kinetic data from these three sources agrees fairly well, but there are differences in the models used to calculate diffusion coefficients. Seguchi employed the 3-D Fick's law diffusion model and used initial and boundary conditions similar to those used in this work (i.e. $R=L/2$ where L is the long period). Seguchi, however, estimated D_a by fitting the 3-D model concentration-predicted profiles to experimental decay data for several PE with various long periods (L=93–151 Å), rather than the half-life method used here. Nonetheless, the $(D_a)_{3\text{-D}}$ value reported by Seguchi, 3.0×10^{-18} cm^2 s^{-1} agrees fairly well with $(D_a)_{3\text{-D}}=2.3\times10^{-18}$ cm^2 s^{-1} estimated in this research.

Shimada's reported diffusivity of 1.1×10^{-21} cm^2 s^{-1} in the crystalline region is over 10 000 times smaller than the values calculated using his kinetic data with the models described above, as given in *Table 4*. Since his kinetic data agrees fairly well with this and previous work, the large discrepancy in D_a must be due to Shimada's modelling of radical migration in the crystalline and amorphous regions as being independent and non-interactive. Shimada assumed that radicals formed in the crystalline interior during irradiation that are trapped there are not permitted to enter the amorphous zones. This description contradicts the generally accepted view that radicals formed in the crystalline region migrate to the amorphous fold surfaces to combine there[2,8–11,17,30]. Shimada's model implies that radicals located in the crystalline zone can only decay by combining with other radicals within the crystalline zone. This would result in a significantly longer mean free path length and thus a lower alkyl diffusivity than obtained by assuming that radicals are free to pass from crystalline to amorphous regions where they rapidly recombine.

CONCLUSIONS

Irradiated PE single crystals were analysed by e.p.r. to determine alkyl radical decay kinetics and estimate alkyl radical diffusivity. A first-order alkyl radical decay constant of 4.3×10^{-5} s^{-1} at 298 K was determined, in agreement with the decay rate of the slow radicals reported in the research of Dole *et al.*[12,16], Seguchi and Tamura[27], and Shimada *et al.*[28]. Alkyl radical migration was modelled using the one, two and three dimensional unsteady state Fickian diffusion equations, yielding diffusivities varying from 10 to 4×10^{-18} cm^2 s^{-1}, respectively, based on a constant migration path length. These values agree to within an order of magnitude with a diffusivity estimated by Seguchi and Tamura[27], but differ greatly from Shimada's value, probably due to an unrealistic assumption in his model regarding lack of communication between radical populations in the crystalline and amorphous zones. A three-dimensional diffusion model is probably more realistic than 1-D or 2-D since a 3-D model more accurately incorporates the crystalline PE morphology and allows a net intramolecular migration process.

ACKNOWLEDGEMENT

The authors are pleased to acknowledge support from the National Science Foundation through NSF grant DMR-75-15205.

REFERENCES

1 Keller, A. *Phil. Mag.* 1957, **2**, 1171
2 Priest, D. J., Keller, A., Martuscelli, E. and Udagawa, Y. *J. Polym. Sci. A-2* 1971, **9**, 1807
3 Ungar, G., Grubb, D. T. and Keller, A. *Polymer* 1980, **21**, 1273
4 Ungar, G., Grubb, D. T. and Keller, A. *Polymer* 1980, **21**, 1284
5 Charlesby, A. *Proc. Roy. Soc.* (*London*), 1954, **A22**, 60
6 Dole, M., Keeling, C. D. and Rose, D. G. *J. Amer. Chem. Soc.* 1954, **76**, 4304
7 Miller, A. A., Lawton, E. J. and Balwit, J. S. *J. Chem. Phys.* 1956, **60**, 599
8 Salovey, R. S. and Keller, A. *Bell System Technical J.* 1961, **40**, 1397
9 Lawton, E. J., Balwit, J. S. and Powell, R. S. *J. Chem. Phys.* 1960, **33**, 405
10 Dole, M. and Cracco, F. *J. Phys. Chem.* 1962, **66**, 193
11 Charlesby, A., Libby, D. and Ormerod, M. G. *Proc. Roy. Soc. Ser. A* 1961, **262**, 207
12 Waterman, D. C. and Dole, M. *J. Phys. Chem.* 1970, **74**, 1913
13 Ormerod, M. G. *J. Polym. Chem.* 1961, **15**, 451
14 Chapiro, A. 'Radiation Chemistry of Polymeric Systems', Interscience, NY, 1962
15 Dole, M. and Bohn, H. *Eur. Polym. J.* (supplement), 1969, 93
16 Dole, M., Wen, W. and Johnson, D. R. *Macromolecules* 1974, **7**, 199
17 Dole, M., Wen, W. and Johnson, D. R. *J. Phys. Chem.* 1973, **77**, 2174
18 Dole, M. and Patel, V. M. *J. Polym. Sci.* 1977, **15**, 907
19 Keller, A. *J. Polym. Sci.* 1962, **62**, 291
20 Peterlin, A., Ingram, P. and Kiko, H. *Macromol. Chem.* 1965, **86**, 294
21 Harrison, I. R. and Baer, E. *J. Polym. Sci., A-2* 1971, **9**, 1305
22 Quenum, B. M., Berticat, P. and Vallet, G. *Polym. J.* 1975, **7**, 277
23 Margrave, J. *J. Polym. Sci. B* (*Lett.*) 1974, **12**, 177
24 Morrison, R. T. and Boyd, R. N. *Organic Chemistry* (2nd Edn.), Allyn and Bacon, Inc., Boston, 1966, p. 184
25 Grubb, D. T. and Keller, A. *Proc. 5th European Congress on EM* 1972, p. 554
26 Grubb, D. T. *J. Phys. E: Scientific Instruments* 1971, **4**, 222
27 Seguchi, T. and Tamura, R. *Reports of Progress in Physics in Japan* 1971, **14**, 565
28 Shimada, S., Hori, Y. and Kashiwabara, H. *Polymer* 1977, **18**, 25
29 Schultz, J. M. *Polym. Mater. Sci.* Prentice Hall Inc., Englewood Cliffs, NJ, 1974
30 Osamu, Yoda, Isamu, Kuriyama and Akira, Odajima *J. Mater. Sci. Lett.* 1982, **1**, 451
31 Hosemann, R., Wilke, W. and Balta Callega, F. J. *Acta. Crystallogr.* 1966, **21**, 118
32 Waite, T. R. *J. Chem. Phys.* 1960, **32**, No. 1, 21
33 Varnell, W. D., Ryba, E. and Harrison, I. R. *J. Macro. Sci.* (*Phys.*) in press